Additive Manufacturing 28 (2019) 344–353

Contents lists available at ScienceDirect

Additive Manufacturing

journal homepage: www.elsevier.com/locate/addma

Single-operation, multi-phase additive manufacture of electro-chemical double layer capacitor devices

Lukas Fieber*, Jack D. Evans, Chun Huang, Patrick S. Grant

Department of Materials, University of Oxford, Parks Road, Oxford OX1 3PH, United Kingdom

ARTICLE INFO

Keywords:
Supercapacitor
Energy storage
EDLC
3D printing
Fused filament fabrication
Direct ink writing

ABSTRACT

Additive manufacturing (AM) may offer a flexible, cost-effective approach to address conventional manufacturing limitations, such as time-consuming, high work-in-progress, multi-step assembly. In principle AM can also allow more novel geometric or even bespoke designs of structural and functional products. However, in terms of energy storage devices such as batteries and supercapacitors, the benefits of AM have not yet been explored to any significant extent. In this paper, a hybrid-AM system, combining low-cost fused filament fabrication (FFF) and direct ink writing (DIW) techniques, has been designed to fabricate supercapacitors (electro-chemical double layer capacitors, EDLCs) in a single, automated operation. The inherent flexibility of the AM process provided an opportunity to address restrictions in geometric form factor associated with conventional planar supercapacitor manufacturing approaches. Functioning, ring-shaped EDLC devices were manufactured in a single, multi-material operation comprising symmetric activated carbon electrodes in a 1M potassium hydroxide (KOH) electrolyte hydrogel. Gravimetric and areal electrode capacitances were 116.4 ± 0.6 F g^{-1} and 599.2 ± 3.0 mF cm^{-2} at 10 mV s^{-1}, with a columbic efficiency of 99.6 ± 0.4% in the as-printed condition. The work aims to accelerate progress towards monolithic integration of energy storage devices in product manufacture, offering an alternative fabrication process for applications with irregular volume/shape and mass-customization requirements.

1. Introduction

Printed power sources are an emerging concept to address conventional manufacturing limitations associated with roll-to-roll slurry casting of electro-chemical energy storage devices, such as expensive multi-step cell assembly and inherent planar form-factor restrictions. Additive manufacturing (AM) ideas and approaches, while not yet penetrating significantly into the energy storage sector, may provide opportunities to address these limitations while allowing direct integration of power-sources into printed products, facile free-form device fabrication and even cost-effective mass-customization [1,2].

1.1. Electro-chemical double-layer capacitors

1.1.1. Supercapacitors: motivation & applications

Electro-chemical energy storage (EES) devices are used in power systems across a wide range of storage time-scales, spanning applications in grid-scale buffering of volatile renewable energy sources using Li-ion or red-ox flow batteries [3], down to representing binary information in microelectronics using chip capacitors [4]. In the pursuit of high-energy and simultaneously high-power EES technologies, supercapacitors have attracted attention because they provide up to 2-3 order higher energy densities than conventional electrolytic capacitors ($\sim 10^{-2}$ Wh kg^{-1}) and have power ($\sim 10^{2}$ W kg^{-1}) and cycling performance ($> 10^{6}$ cycles) superior to ion-batteries [5].

1.1.2. The primary charge storage mechanism of supercapacitors

The various types of capacitors may be differentiated based on their primary charge storage mechanism: (a) *electro-static* – physical adsorption of electrolyte ions onto a polarized electrode surface to satisfy local electro-static equilibrium in an electric double layer (EDL); (b) *pseudocapacitive* – reversible faradaic surface reactions giving rise to a capacitive term i.e. charge ∝ electric potential; and (c) *chemical* – bulk or intercalation reduction and oxidation reactions to satisfy Nernstian thermodynamic equilibrium [6,7]. Electro-chemical double layer capacitors (EDLCs) predominantly store energy in an electro-static manner and are considered in this work. However in principle, the manufacturing approach that is demonstrated could be applied to other, more complex EES devices, such as ion-batteries.

* Corresponding author.
E-mail address: lukas.fieber@ccc.ox.ac.uk (L. Fieber).

https://doi.org/10.1016/j.addma.2019.05.001
Received 5 February 2019; Received in revised form 11 March 2019; Accepted 2 May 2019
Available online 14 May 2019

1.1.3. EDLC architecture & functionality

Conventional EDLCs consist of symmetric (identical anode and cathode), high surface area porous electrodes separated by an ion permeable but electrically insulating separator, immersed in a liquid or gel electrolyte. The primary functions of the key components are: (a) *porous electrode* – to provide maximum ion-accessible surface area for electro-static charge storage while retaining electrical conductivity, and chemical as well as mechanical stability throughout cycling; (b) *separator* – to electrically insulate electrodes from one another while allowing electrolyte ions to shuttle between the electrodes during charge/discharge; (c) *electrolyte* – to provide a source of ions allowing the local electro-static equilibrium to be satisfied at the electrode surfaces; (d) *current collector* – to supply electrons to and from an external circuit to polarize the electrodes; and (e) *housing* – to encapsulate the complete cell arrangement, to provide mechanical protection, and to prevent electrolyte leakage.

1.1.4. Recent focus in advancing EDLC manufacture

The majority of work concerning EDLC manufacturing has addressed the synthesis of cost-effective, high-surface area electrode materials [8,9], the improvement of interfaces between, for example, the electrode and electrolyte [10] i.e. interfacial resistance, as well as advancements in electrolyte bio-compatibility and safety [11,12]. The slurry casting based manufacturing and assembly process itself however, has received surprisingly little attention [13] and has therefore remained largely the same for many years [14].

1.1.5. Current EDLC manufacturing & materials

Electrodes are usually manufactured in a roll-to-roll process synonymously known as either *doctor blading*, *slurry casting* or *slot-die coating*. A slurry containing particulates of the high surface area active material (e.g. activated carbon with area up to 2000 $m^2\ g^{-1}$), electrically conductive additives (e.g. ultra-fine carbon black particulate) and a binder (e.g. 10 wt% polytetrafluoroethylene (PTFE)) in a fugitive solvent (e.g. N-Methyl-2-pyrrolidone (NMP)) is deposited continuously onto a moving current collector (e.g. aluminum foil, 10 to 30 μm thick) with the slurry smoothed to a constant pre-set electrode thickness (50 to 150 μm) by a passing blade [14]. Once the electrodes have dried, usually along a drying tunnel on a conveyor, cells are assembled in a multi-step process involving calendaring, cutting/foiling, winding or stacking, electrolyte injection, sealing, welding, heat pressing and aging [2,15].

1.1.6. Problems with the current manufacture of EDLCs

Supercapacitor manufacture is mature and highly productive but there are inherent limitations including: (a) restrictions in geometric form factor and device architecture [13]; (b) costly multi-step assembly inducing long lead-times and high up-front capital investments [15]; and (c) the need for performance hindering binders to hold the porous, particulate based electrode together and onto the current collector [16]. Overcoming these limitations may further help exploit the attractive features of supercapacitors and secure their use in a wider range of emerging applications [17].

1.2. Additive manufacture of EDLCs

1.2.1. General concept of AM

AM can be defined as *any process of joining materials to make parts from 3D model data, usually layer upon layer, in contrast to subtractive manufacturing and formative manufacturing methodologies* [18]. AM has been suggested to have the potential to revolutionize manufacturing in many fields [19] by allowing shortened design and production cycles [20], and through the manufacture of complex geometries without the restrictions of conventional manufacturing methods such as tool-tip accessibility for internal features.

1.2.2. Current state of AM

The majority of AM research has focused on single alloy, polymer or ceramic monoliths of relatively complex shape [21]. Only recently have functional, multi-material arrangements been studied in earnest, and AM demonstrators of functioning multi-material devices are rare [22].

1.2.3. The promise of AM

Whilst acknowledging that the principal challenge in manufacturing EDLCs lies in economically fabricating controlled structures over many length scales (nano-porosity of the active particles [nm] through to semi-continuous electrode lengths [m]), the spatial and temporal control of material deposition in AM processes may facilitate [13]: (a) unprecedented control and exploration of new geometric form factors [23] as well as the ability to deposit complex shaped electrodes on e.g. conformal substrates (which themselves may be additively manufactured) achieving high-aspect ratio electrode configurations for shortened ion diffusion paths, including periodic or interdigitated architectures [24]; (b) process flexibility in terms of material feed-stock properties (e.g. paste, powder, laminate, filament, suspension) and greater speed that may allow facile prototyping and testing of novel materials combinations; (c) cost-effective, decentralized manufacturing [25] while minimizing material waste and abolishing the need for part-specific tooling; and (d) progress towards monolithic integration and mass customized power sources such as on-chip printing of energy storage devices directly into crowded micro-devices [2].

1.2.4. Review of AM for EDLCs

There have been only limited reports of the manufacture of EDLC components or even entire cells using AM [1,13,26]. Material extrusion additive manufacture (MEAM) processes such as FFF [27] and DIW [28,29] are among the most widely used processes, partly due to their relatively low capital and running costs, broad range and quickly expanding palette of processable materials, along with generally no need for significant heat input during processing or chemical post-treatment of printed parts [30,31].

1.2.5. Fused filament fabrication

In FFF a continuously fed thermoplastic filament is liquefied by heating (180–250 °C) in a print head, extruded through a nozzle (∅0.15–1.2 mm) and solidified upon deposition onto a temperature controlled building platform (20–120 °C) to form three dimensional (3D) objects in a layer-by-layer manner. Process parameters such as print speed [$mm\ s^{-1}$], extrusion temperature [°C] and print path as well as feedstock material properties such as melt viscosity [Pa s] and elastic modulus [Pa] significantly influence the fabricated quality (tolerance, pores, surface finish, distortion, etc.) in a complex, and usually difficult to predict, manner [20,30].

1.2.6. Direct ink writing

DIW is based on the micro-dispensing (pneumatic or electric actuation) of materials as a viscous liquid *ink* through a narrow orifice (∅0.1–250 μm) onto the aforementioned building platform [29,32]. The main challenges lie in the non-trivial ink formulation and its associated rheology (e.g. shear-thinning), as well as the drying and fusing behavior of layers by evaporation, in which surface tension effects play a key role, or chemical changes such as cross-linking [33]. The versatility, high-loading of active material and reduced risk of nozzle-clogging, when compared to for example ink-jet printing, makes DIW attractive for AM of EDLCs. Key process parameters include volumetric flow rate [$mm^3\ s^{-1}$], dispensing height [μm], solvent vapor pressure [Pa] and nozzle diameter [μm] [32,34].

1.3. Current work

This paper seeks to demonstrate how existing EDLC materials can be used in MEAM processing techniques (FFF and DIW) to fabricate or *print*

functioning, form-factor free electro-chemical energy storage devices in a single operation. The objective is not to achieve energy storage behavior (e.g. gravimetric capacitance, cost, lifetime) that is superior to the mature slurry cast electrodes and devices commercially available, but to demonstrate encouraging performance in a novel form factor impossible by current approaches. Although surprisingly good energy storage behavior has been achieved, the key insight is that AM of supercapacitors/EDLCs, and perhaps other EES devices such as Li-ion batteries, is both feasible and attractive.

2. Materials and methods

2.1. Multi-material AM

A bespoke, hybrid multi-material AM machine was designed, built and commissioned allowing for up to 9 complementary AM and *in-situ* characterization techniques to be automated in a single, numerical control (NC) operation. The machine interprets conventional g-code (RS274) protocol through a modified repetier based firmware running on a 8-bit micro-controller (ATmega2560). All primary mechatronic and thermal systems are proportional-integral-derivative (PID) controlled and tuned using the Ziegler Nichols method [35] to improve response time and minimize overshoot. Cartesian motion at up to 40 mm s^{-1}, acceleration up to 60 mm s^{-2} and jerk up to 5 mm s^{-1} allows printing and characterization in an envelope of a 200 mm cube, with spatial resolution of ± 3.4 μm and ± 1.5 μm in the horizontal and vertical planes respectively. For the purpose of printing EDLCs the machine was fitted with at least two FFF modules and three DIW modules as shown schematically in Fig. 1.

2.2. Materials & ink preparation

Functional inks were prepared on the day of EDLC manufacture as outlined hereafter. Unless otherwise stated, chemicals were sourced from Sigma-Aldrich UK and, where possible, industry standard materials were used.

2.2.1. Electrode

A two-step mixing process was adopted from [36], given the typically cuboid shape of commercial activated carbon particles for supercapacitors. A water-insoluble binder was chosen to allow for the facile fabrication of aqueous electrolyte EDLCs in atmospheric conditions, and the binder content was chosen to maximize electro-chemical performance while preserving electrode stability [37]: (1) mixing of activated carbon (YP80F from Kuraray, Germany), conductive additive (carbon black 99.9% from Alfa Aeser, UK), a solvent with high boiling point (NMP CAS 872-50-4) and a low boiling point (isopropyl alcohol (IPA) CAS 67-63-0) in a weight ratio of 0.8:0.2:2.5:7.5 at 250 rpm for 20min; (2) addition of a binder (polyvinylidene fluoride (PVDF) CAS 24937-79-9) dissolved in a solvent (NMP) to the slurry in a weight ratio of 0.05:2.5:11 and mixing at 250 rpm for 20 min. A zirconium (ZrO_2) pot with 8 ZrO_2 balls (∅1cm) was used in a planetary ball mill (Pulverisette 6 from Fritsch GmbH) to prepare the slurry. The electrode slurry was back-loaded into a syringe (Nordson EFD Optimum 3cc barrel) ready for DIW.

2.2.2. Electrolyte hydrogel

A thickening agent (polyvinyl alcohol (PVA) CAS: 9002-89-5) was mixed with de-ionized water and a salt (potassium chloride (KCl) CAS: 7447-40-7) in a weight ratio of 5:100:14.9 at 90 °C, 400 rpm for 1 h to synthesize a 1M hydrogel electrolyte. The hydrogel was cooled to room temperature and back-loaded into a syringe (Hamilton 1002RN 2.5mL barrel) ready for DIW.

2.2.3. Current collector

A commercial conductive ink based on silver (Ag) nano-particulates

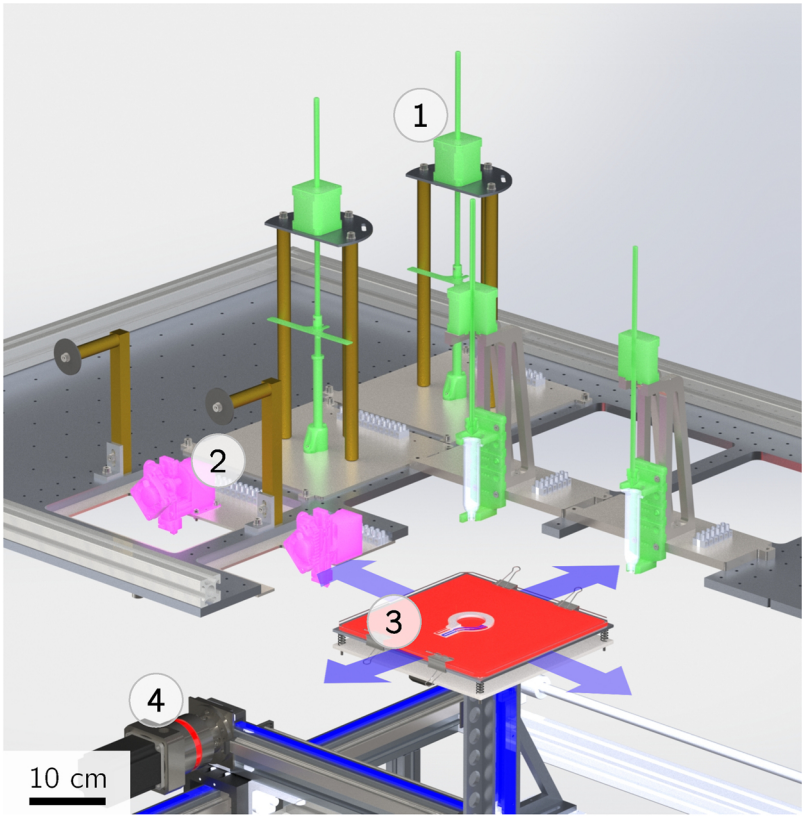

Fig. 1. Photorealistic cross-section of the bespoke multi-material, hybrid-AM machine: (1) DIW and (2) FFF modules, (3) heated bed (< 150°C) acting as substrate for printed EDLCs and (4) interplanetary 10:1 reduction gear-boxes allowing spatial resolution of ± 3.4 μm.

(IINK-SSX from IIMAK, USA) was back-loaded into a syringe (Nordson EFD Optimum 3cc barrel) ready for DIW.

2.2.4. Housing

A polypropylene (PP) filament (Centaur PP from FormFutura, The Netherlands) was used for FFF fabrication of all of the supercapacitor housing elements. The filament was dried at 50 °C for > 5 h prior to printing.

2.3. EDLC cell design & sequential manufacture

2.3.1. Machine code generation

Complete EDLC cells were designed as multi-part assemblies in computer aided design (CAD) software (SolidWorks 2017) before being exported as individual stereolithography (STL) files with respect to a common origin. Open source slicing software (Slic3r v.1.3.0) was used to generate a basic layer-by-layer, machine interpretable g-code file, which was thereafter modified (MatLab R2018a) to reflect calibration values for the hybrid-AM machine, alongside module-dependent routines for tool changes including syringe purging prior to DIW processes, accounting for drying-times where needed, and prevention of tip-clashes. A custom printing host was developed for communicating with the hybrid-AM machine, incorporating debugging and live monitoring functionality, as well as for automating the g-code generation process.

2.3.2. Manufacturing sequence & print parameters

Entire EDLC (supercapacitor) devices were manufactured as follows, with an example geometry and manufacturing sequence schematically depicted in Fig. 2: (1) FFF of 2 rectilinear, orthogonal base layers (each 200 μm high, 100% infill), as well as external and internal walls (200 μm high, 800 μm and 400 μm wide respectively), to assist (2) DIW of the current collector ink which was (3) dried at a 80 °C bed temperature for 100 s yielding typical current collector thicknesses of 20 μm. Thereafter (4) FFF of housing walls sufficiently high (600 μm) for (5) DIW of an electrode layer, before (6) drying of the electrode at a bed temperature of 70 °C for 500 s yielding typical electrode layer thicknesses of 40–120 μm depending on the specified extrusion multiplier. Steps 5 and 6 were repeated for the desired number of electrode layers before, (7) FFF of the housing walls to allow for, (8) DIW of the electrolyte hydrogel before finally (9) sealing of the device using FFF. The nozzles were tapered (PE) tips ∅0.58 mm for electrode and current collector inks, a tapered PE tip ∅1.6 mm for the electrolyte hydrogel and a hardened steel ∅0.4 mm nozzle with a titanium hot-end for FFF of the housing.

2.4. Cell characterization

2.4.1. Electro-chemical performance evaluation

To evaluate key electro-chemical performance parameters, cyclic voltammetry (CV), constant current charge/discharge (CCCD) and electro-chemical impedance spectroscopy (EIS) measurements were carried out on as-printed, full-cell EDLCs using a potentiostat (Gamry 600), following the guidelines given in [38].

CV - The rate performance of printed EDLCs was evaluated by applying a linear voltage ramp across working and counter electrodes over an electric potential window $\phi_e \in [V_0, V_1]$ for 10 cycles at constant scan rates $\nu \in [5, 10, 25, 50, 100]$ mV s^{-1}. The current response $i(V)$ of the cell was recorded where $V_0 = 0$ V and $V_1 = 1$ V such that all components remained within their electro-chemical stability window (ESW). From (1), the total cell capacitance C_{cell} was estimated by trapezoidal numerical integration (MatLab) and normalized by active material mass, electrode footprint area and number of electrodes.

$$C_{\text{cell}} = \frac{1}{2(V_1 - V_0)\nu} \oint_{V_0}^{V_1} i(V)\mathrm{d}V \tag{1}$$

The efficiency of charge-discharge cycles was evaluated by comparing the electrons required to charge Q_{charge} and received during discharge $Q_{discharge}$, expressed as $\eta = Q_{discharge}/Q_{charge}$. Cycling performance was investigated at $\nu = 25$ mV s^{-1} by evaluating the columbic efficiency of charge and discharge cycles, as well as capacitance retention over 250 cycles.

CCCD - After conditioning the printed EDLC cells to 0V for > 60s, a constant current of $i \in [0.5, 1, 2]$ Ag^{-1}, normalized to the total mass of active material in the EDLC cell, was applied to the cell to charge to a working potential of $\phi_e > 1$ V and then immediately, without dwelling, discharge to a working potential of $\phi_e < 0$ V. The steady-state drop in working potential ΔV_{ss} was evaluated by extrapolating the 2 to 5% discharge states to the moment of current reversal $\Delta i = 2|i|$. An interpretation of the electrical series resistance (ESR) was derived following a conventional method ($ESR_{CCCD} = \Delta V_{ss}/\Delta i$) [38].

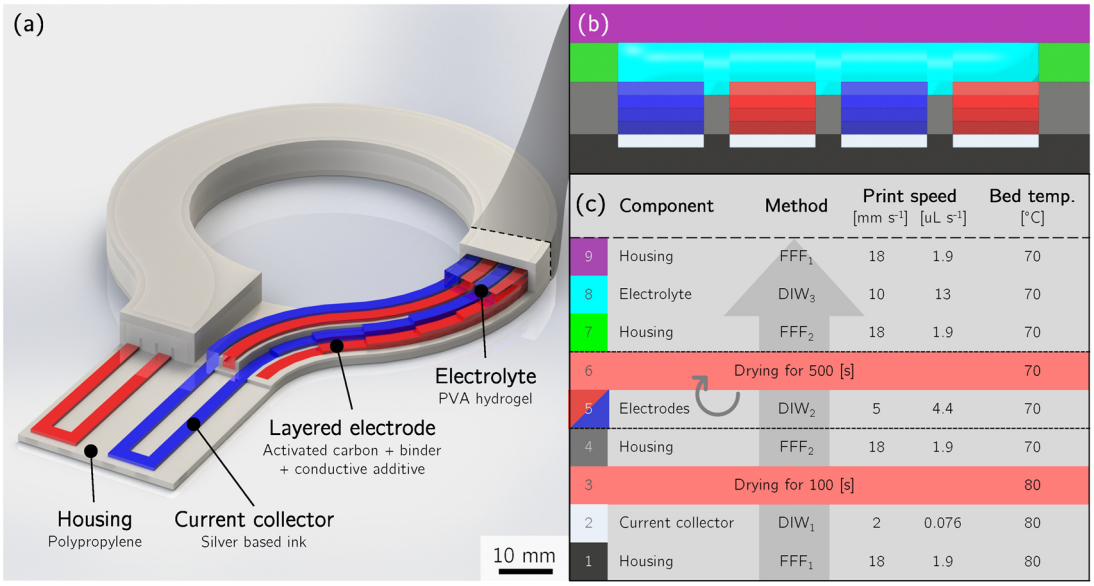

Fig. 2. (a) Isometric render of the demonstration AM EDLC highlighting the unusual geometric *ring* form factor and functional elements, (b) cross-section of the EDLC orthogonal to the print direction, depicting the arrangement of different color-coded materials, and (c) the corresponding color-coded table showing the manufacturing sequence and a selection of key processing parameters.

EIS - An oscillating, time harmonic excitation wave with amplitude $V_a = 5$ mV was applied to the EDLC cells at open circuit voltage ($V_0 = 0$ V) over a range of frequencies $f \in [10^{-2}, 10^{6}]$ Hz according to $V_i = V_0 + V_a \sin(2\pi f \times t)$. The temporal current response $i(t)$ of the EDLC was recorded and using *Ohm's Law* in complex form $V \propto [Re(Z) + Im(Z)]$, attenuation $|Z|$ and phase shift θ as function of frequency were recorded. Under the assumption that the electro-chemical system behaved pseudo-linearly over the small excitation wave, parameters including the ESR were evaluated following [39]. A Randles equivalent circuit was fit to EIS spectra to determine the Warburg diffusion coefficient.

2.4.2. Physical characterization

Electrode weight - 250 μL of electrode ink was dispensed into a petri dish of known weight, heated above the boiling point of all solvents 250 °C and dried for > 1 h. The net dry-weight of active material (mg μL $^{-1}$) was used to estimate the electrode weight from relevant commands in the machine code i.e. the weight of active material in a device was estimated from the calibration of the weight dispensed per unit volume.

Rheology - The rheology, in particular the shear-thinning behavior of electrode inks, was characterized and optimized using a rheometer (Ametek Brookfield DV2-T). The cone spindle set-up was selected to: (a) apply DIW relevant shear-rates $\dot{\gamma} \in [0.5, 50]\ s^{-1}$; (b) allow small sample sizes < 1 mL to be evaluated; and (c) allow the use of a rheological continuum assumption [40], that is, the particle loaded ink can be considered pseudo-homogeneous.

Electrode morphology - The morphology of as printed electrodes was investigated by scanning electron microscopy (SEM) (JEOL JSM-6500F). A cross-section of an EDLC printed without electrolyte, and coated with 5nm of platinum (Pt), was used to investigate the interfaces between functional components, alongside the evaluation of electrode and current collector thickness. Whitelight confocal microscopy (NanoFocus μSurf) was used for 3D surface measurements of electrodes and printed features over areas of 1.5 × 1.5 mm with depth ranges of up to 250 μm.

Printed features - Printed features were observed using an optical microscope (Leica M165C). X-ray tomography (XRT) (North Star Imaging Imagix 150 kV) was used to investigate the spatial arrangement of printed features within complex 3D EDLC cells at 51 μm voxel size. For improved contrast and visualization purposes, lithium ferrophosphate ($LiFePO_4$), acting as a contrast agent principally due to attenuation by iron (Fe), was added to the electrode ink and an aluminum (Al) filter was placed in front of the X-ray source to partially absorb low energy photons. The surface roughness and thickness of printed features was evaluated using the aforementioned confocal microscope.

3. Results and discussion

Functioning EDLC devices with a variety of form factors, cell configurations and electrode thicknesses were fabricated in a single, automated hybrid FFF-DIW manufacturing operation. The fabrication process dismissed the need for any cell assembly and packaging steps, potentially allowing for direct integration into 3D printed systems and components. The devices were typically fabricated in under 30 min. Key materials and processing considerations for repeatable AM of EDLCs are discussed in Appendices A to D. Findings presented here focus on (i) the characterization of as-printed devices and (ii) exploration of electrode thickness, cell configuration and geometric form factor.

3.1. Characterization of as-printed EDLCs

Physical and electro-chemical characterization was conducted on as-printed EDLC devices fabricated using the single operation hybrid FFF-DIW approach outlined in Section 2.3. Fig. 3a schematically shows the *linear EDLCs* that were fabricated in order to assess basic supercapacitor behavior (and for process optimization) before the more complex multi-layer *ring* EDLCs in Fig. 2 were fabricated.

3.1.1. Physical characterization

Fig. 3 shows SEM micrographs of (b) a cross-section of the *linear EDLC*; (c) and (d) the interfaces between the PP housing – Ag-based current collector – carbon (C)-based electrode. Fig. 3b shows how K^+ and OH^- in the electrolyte hydrogel pass between the anode and cathode during operation, with short circuit avoided by the dividing *wall* of housing between the electrode tracks. Note the *bridge* printing of the housing by FFF over the top of the electrolyte hydrogel to seal the cell (see Appendix D). Printing parameters were selected to achieve electrode thicknesses of 100 ± 10μm, similar to the thickness of commercial EDLCs, and current collector thicknesses of approximately 25 μm. Note the minimum *width* of features/components fabricated by DIW (e.g. current collector and electrode) was limited by the choice of DIW nozzle diameter (i.e. ∅0.58 mm reported here) and ink spreading behavior (determined by surface energy and substrate properties). Through the addition of fugitive solvents to dilute the functional inks, there was no observable lower limit (< 5 μm) to the minimum layer thickness, other than ultimately the size of deposited particulates. The difference in morphology, from a relatively smooth, monolithic housing to the micron sized Ag-flakes in the current collector led to poor contact adhesion between these two elements. Although this is likely to have little effect on the electro-chemical performance of a cell, as the housing is an inactive component, improving the current collector-housing interface should be addressed for applications where mechanical integrity is required over long life-times. Fig. 3d shows how Ag-flake based current collector was completely dried prior to DIW of the electrode (no intermixing). The primary particles of the activated carbon in the electrode and the Ag-flakes had comparable dimensions that facilitated a well-matched inter-locking C/Ag interface.

3.1.2. Electro-chemical characterization

CV - Fig. 4a shows cyclic voltammograms for an as-fabricated *linear EDLC* as a function of scan rate from 5 to 100 mV s^{-1}. The plots were quasi-rectangular and indicate acceptable EDLC-type behavior (ideal EDLCs show classic rectangular cyclic voltammograms). Deviations from ideal performance arose due to internal resistances, and possible underlying non-reversible chemical reactions, the nature of which could not be resolved by similar tests on various materials in isolation but probably relate to Ag-ink/potassium hydroxide (KOH) hydrogel reactions. Nonetheless, their contribution was vanishingly small. By integration of the data in Fig. 4a, the gravimetric electrode capacitance was 116.4 ± 0.6 F g^{-1} at 10 mV s^{-1} based on the total weight of active material, activated carbon (YP80F) and conductive additive (carbon black). Note that it was not possible to weigh the amount of active material in the device directly, and was instead estimated on the volume dispensed and prior calibration. The areal and volumetric electrode capacitance was 599.2 ± 3.0 mF/cm^2 and 61.7 ± 0.6 mF/mm^3 at a scan rate of 10 mV/s, normalized by electrode foot-print area and electrode volume respectively. The devices showed cycling efficiency η of 99.6 ± 0.4% over all tested scan rates and capacitance retention of 97.1% over 250 cycles at 25 mV s^{-1}. The performance demonstrated is comparable to reported symmetric carbon-carbon EDLCs [6,41].

CCCD - Fig. 4b shows the corresponding galvanostatic charge/discharge behavior at 0.5, 1 and 2 A g^{-1}. The inset shows the ESR_{CCCD}, often referred to as *IR* drop on voltage reversal, which was estimated at 3.2 Ω at 1 A g^{-1}. Otherwise the profiles were near-linear, showing good capacitor-only (electro-static charge/discharge) behavior, although once again with a slight deviation from linearity suggestive of possible minor underlying side-reactions.

EIS - Fig. 4c shows the EIS spectrum of a *linear EDLC* prior to cycling. A Warburg diffusion coefficient of 0.8, and an ESR of 13.2 Ω at 1 kHz was estimated. The relatively low diffusion coefficient, when compared to liquid-electrolyte cells, which may be close to the ideal

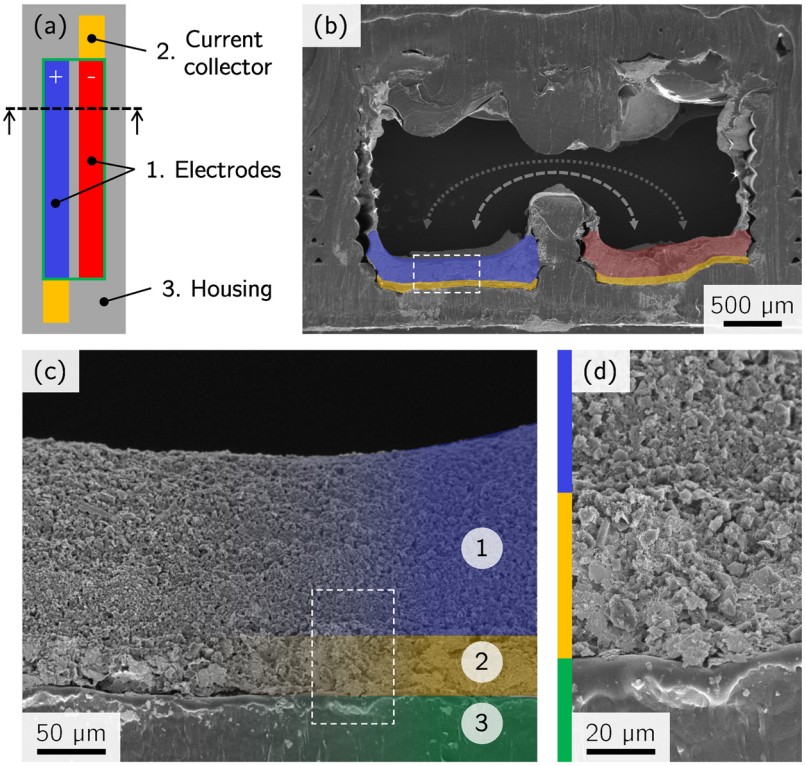

Fig. 3. (a) Color-coded schematic of functional supercapacitor components in the *linear EDLC* configuration for physical and electro-chemical testing, (b) SEM micrograph highlighting the ion diffusion paths between electrodes in a cross-section, (b,c,d) show the color-coded functional elements at different magnifications including (1) the C-based electrodes and (2) the Ag-based current collector fabricated by DIW, as well as (3) the PP housing fabricated by FFF.

coefficient of 1.0, can be explained by the use of a thickening agent (PVA) in the electrolyte hydrogel to achieve AM processability, as well as the relatively long ion diffusion paths (see Fig. 3b) in the printed cells.

3.2. Cell configuration

The increased geometric flexibility inherent in AM processes opens a multitude of possibilities, with a vast design and parameter space, and as such the following section is by no means exhaustive and serves only to indicate what is possible by AM of energy storage devices by focusing on (i) thick electrodes, (ii) parallel cell arrangements, and (iii) form-factor free EDLC fabrication.

3.2.1. Thick electrodes

Ion mobility within thick electrodes - The electrode DIW extrusion multiplier was doubled to increase the dried electrode thickness, from 97 ± 4 to 180 ± 5 µm, for a batch of *linear EDLCs* (Fig. 3a). Fig. 5a shows the resulting Nyquist diagram from EIS now with a lower gradient Warburg element for the thicker electrode (180 µm) (an extended, comparatively shallow EDL formation slope), presumably due to lengthened ion-diffusion paths within the thicker electrodes. The equivalent electrode resistance, including the current collector resistance contributions, increased from 12.8 to 16.1 Ω (+26%) when approximately doubling the electrode thickness. This indicated that the principal resistance was probably due to the current collector-electrode interface (which was unchanged). The thicker electrodes also undermined rate performance, as shown in Fig. 5b. The columbic efficiency was not affected significantly.

3.2.2. Parallel cell arrangements

Internal resistance - Fig. 6a shows photographs and cross-sectional schematics of *linear EDLCs* with 1 pair of electrodes (device 1) and 2 parallel pairs of electrodes (device 2). The EIS spectra, shown in Fig. 6b, revealed that the internal resistance of the device with 2 pairs of electrodes (device 2) reduced to approximately a third of the device with 1 pair of electrodes (device 1), from 12.8 to 4.1 Ω, and not simply to a half which was observed when connecting two devices with 1 pair of electrodes in parallel (Kirchoff's law). Assuming that the electrode resistance was unchanged in both arrangements, since electrodes were fabricated using identical processing parameters, this reduction in internal resistance can be explained by the existence of a third set of ion diffusion pathways in device 2, schematically shown in the cross-sections of Fig. 6a.

Rate performance - The gravimetric capacitance at relatively slow charge-discharge speeds ($\nu < 10$ mV s^{-1}) did not alter significantly, as expected for quasi steady-state systems where the EDL is fully saturated. However, due to the significant reduction in overall electrolyte resistance, the performance of the supercapacitor with 2 pairs of electrodes (device 2) was notably superior to the device with only 1 pair (device 1) when the scan rate was increased. The increased capacitance, indicated by a larger area enclosed by the cyclic voltammograms and highlighted by (i) in Fig. 6d, was due to the larger available surface area (more active material) in device 2. The improved rate performance, indicated by (ii) in Fig. 6d was likely a result of the shortened average ion diffusion paths in the bulk electrolyte. At fast charge-discharge rates ($\nu > 100$ mV s^{-1}) both cell arrangements were only able to utilize a fraction of the theoretical maximum capacitance due to ion mobility limitations in the viscous electrolyte.

3.2.3. Form factor free EDLC fabrication

An arbitrarily shaped 3D *ring EDLC*, impossible by conventional means, was fabricated in a single manufacturing operation, through the sequential manufacture of 4 and 2 electrodes (see Fig. 7a, individual manufacturing steps outlined in 2.3). The fully functional device was fabricated in 32 min. Through extension of this 3D fabrication approach, the geometric permutations available are endless and may offer interesting solutions for applications with irregular volumes, for example in medical implants, aerospace, defence and satellite applications. XRT scans (see Fig. 7b) confirmed that the spatial arrangement of printed EDLC sub-components matched their intended location, with the relatively X-ray absorbing Ag based current collectors and $LiFePO_4$

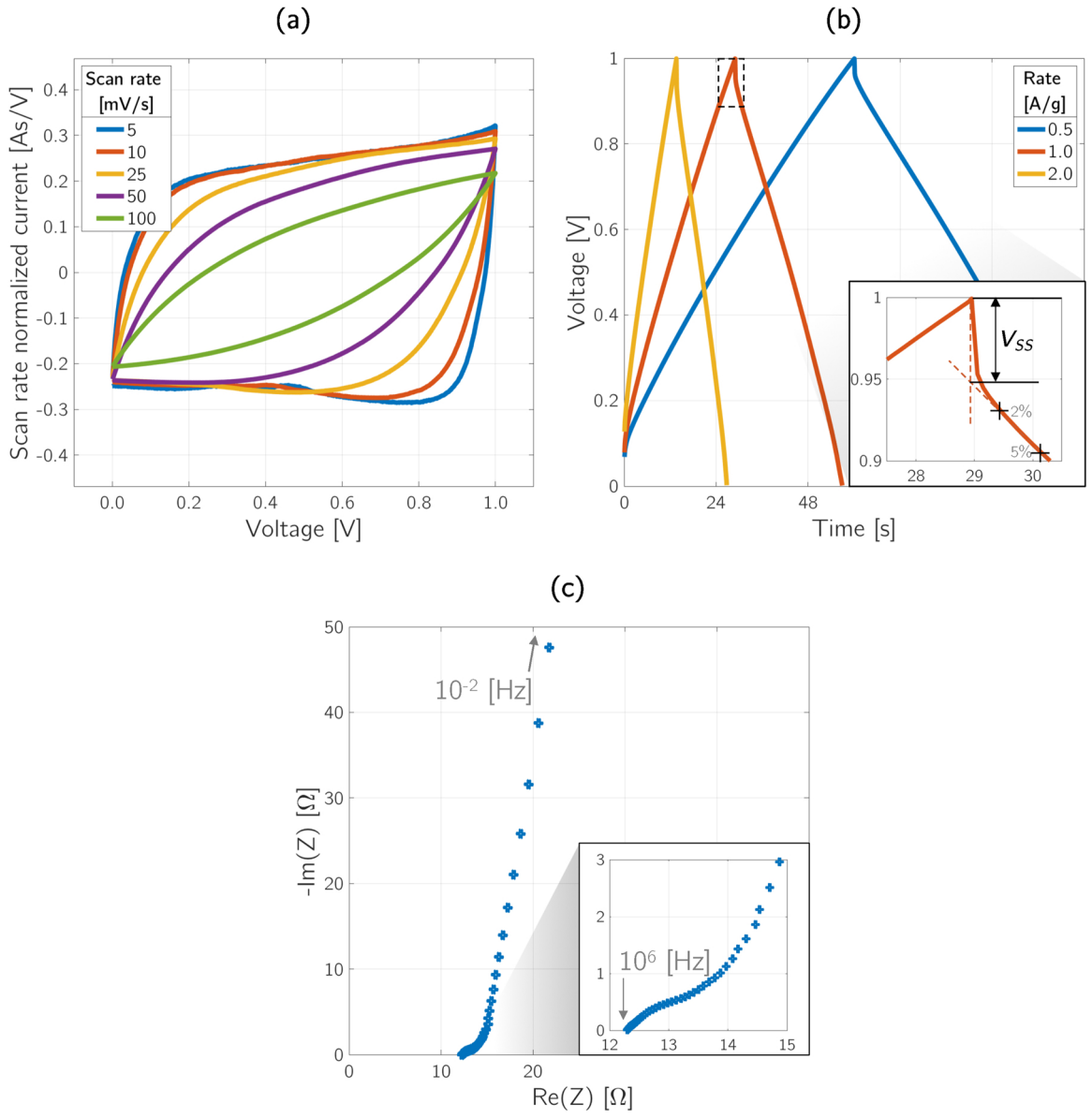

Fig. 4. Electro-chemical performance of as printed, single cell EDLCs showing (a) rate performance from CV curves, (b) CCCD profiles and (c) a EIS spectrum.

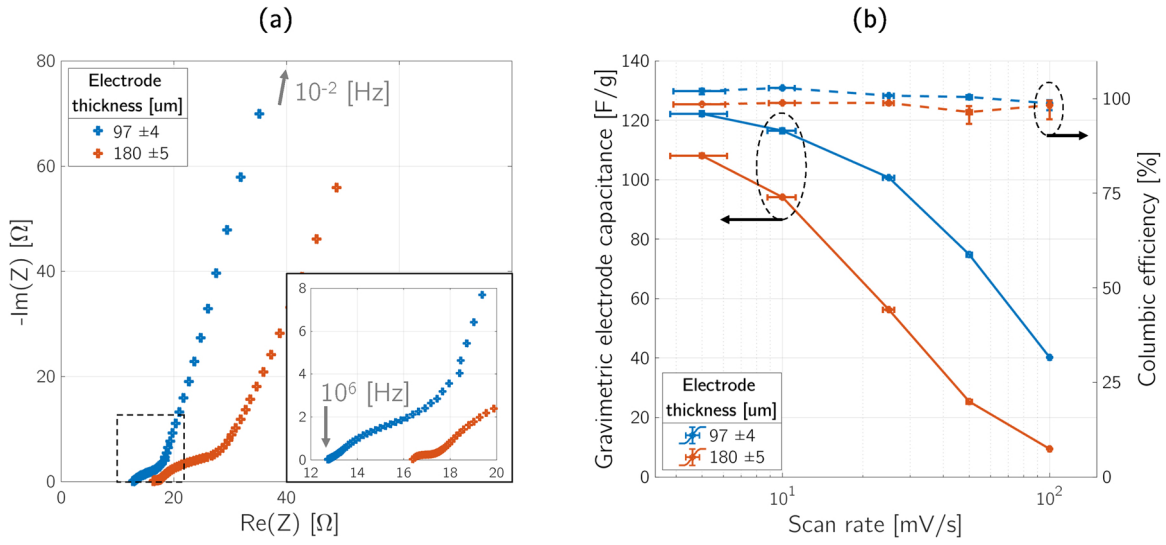

Fig. 5. Effect of electrode thickness on electro-chemical performance in an AM *linear EDLC*: (a) nyquist plot of EIS spectra and (b) rate performance.

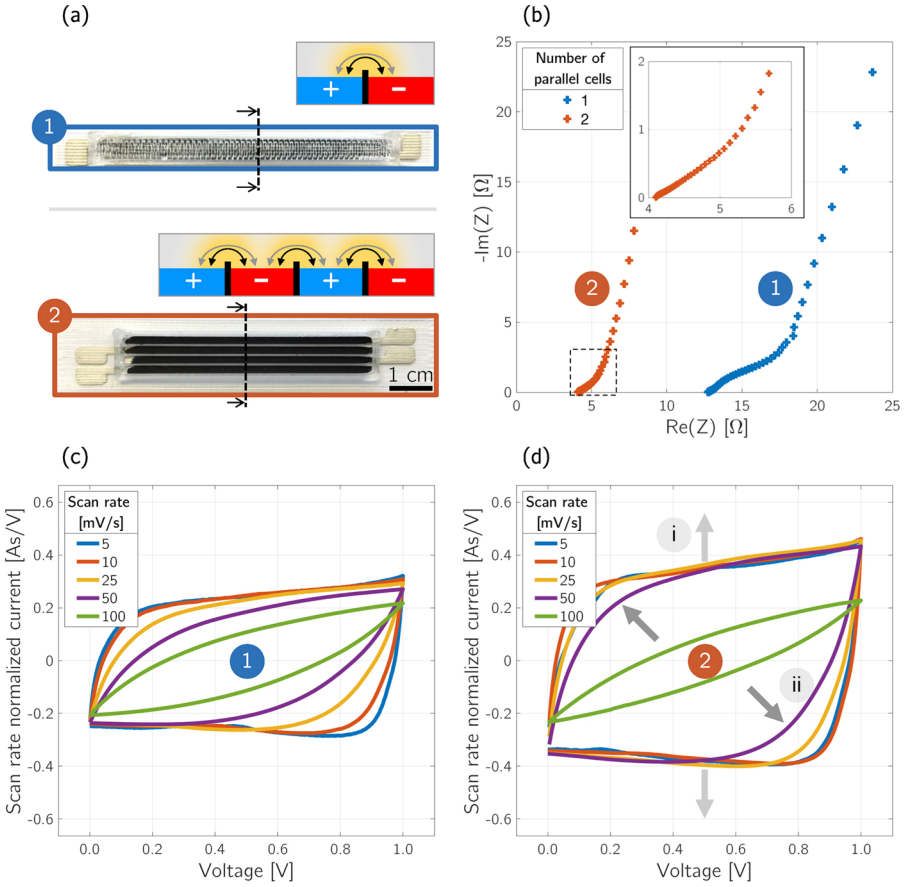

Fig. 6. Electro-chemical performance of a 2-electrode *linear EDLC* (device 1) and a connected, 4-electrode *linear EDLC* (device 2): (a) photographs of a completed, enclosed device 1 and incomplete open device 2 revealing the electrode arrangement of device 2, alongside cross-sectional schematics highlighting the ion diffusion pathways, (b) Nyquist plot of EIS spectra, (c) CV rate performance for device 1 and (d) CV rate performance of device 2 showing the increased capacitance (i) and improved rate performance (ii) of a multi-cell arrangement.

containing C-based electrodes strongly resolved by X-ray adsorption contrast.

4. Conclusion and outlook

4.1. Impact & applications

AM for the fabrication of energy storage devices, such as supercapacitors may be a promising approach for high-value, niche applications where maximizing the utilisation of irregular volumes becomes desirable (e.g. powered miniature devices including medical micro-implants). Furthermore the prospect of assembly-free, monolithic integration of printed energy storage devices in, for example, crowded micro-devices or *on-chip* applications, as well as the facile, lab-scale assessment of unconventional materials combinations and device architectures make the pursuit of fabricating functional devices through

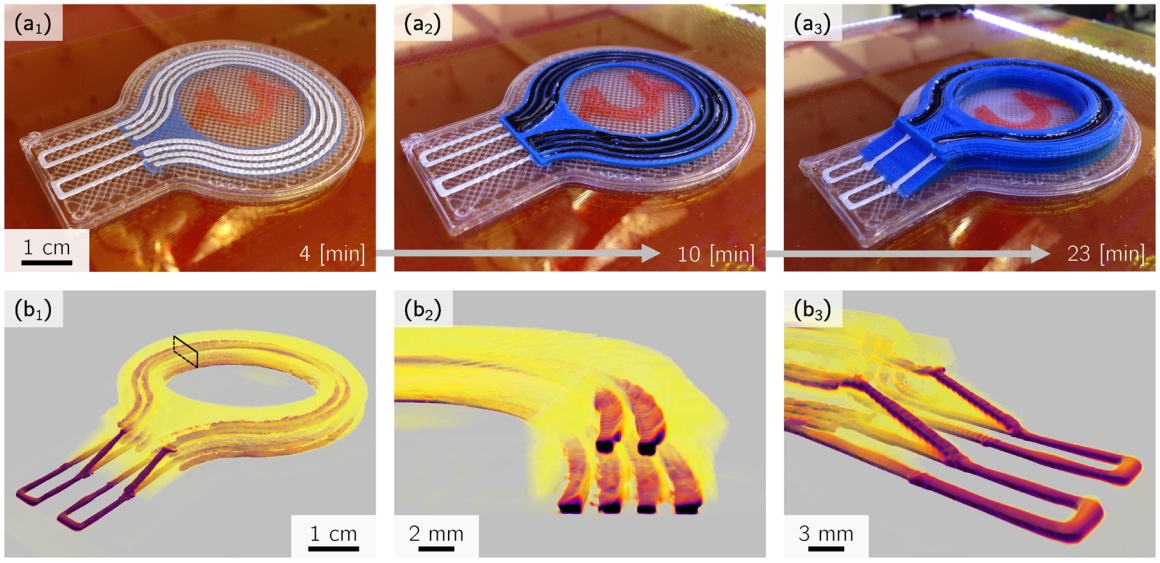

Fig. 7. (a) Photographs of sequential manufacture and (b) XRT renders of 3D spatial arrangement of EDLC components. (a_1) Housing base layer (FFF) and current collectors (DIW), (a_2) electrodes (DIW) in cavities, (a_3) stacking of printed EDLCs,(b_1) complete device, (b_2) cross section showing stacked EDLC cells and (b_3) current collector bridge connecting stacked cells.

AM techniques worthwhile. AM of energy storage devices may provide opportunities in new decentralized manufacturing solutions, with emphasis on material waste minimization and reduction in part specific tooling requirements. However, in the field of mass-market, ultra high area coated electrodes for conventional supercapacitor device fabrication it is unlikely that AM will be able to rival conventional manufacturing processes in terms of economic viability, throughput and efficiency.

4.2. Work achieved

We have demonstrated a novel, single-operation manufacturing process to fabricate fully functioning form-factor free supercapacitor/EDLC devices using a hybrid, multi-phase AM approach. Materials and processing considerations were discussed in detail, fabricated devices characterized and some indicative experiments of how the inherent flexibility in AM processes may be used to explore a previously unachievable geometric parameter space were shown.

4.3. Future research

Remaining challenges in the field of multi-material, multi-phase AM include: (a) greater understanding of the processing science (e.g. rheology, surface/interfacial energy, drying dynamics) governing individual MEAM techniques, alongside (b) insight into the interaction of materials in hybrid-AM systems, (c) extension of the printable materials palette to advanced functional materials, and (d) in-operation quality control techniques for responsive process development. Specifically with respect to AM of energy storage devices, the development of printable separators (ion permeable, electron insulating) would allow for designs that facilitate shorter, more efficient ion diffusion pathways while allowing more freedom for the fabrication of fully/arbitrary 3D cell configurations. The ability to control the surface energy of FFF extrudates and DIW inks would allow engineering of the many interfaces between inks and polymers that are implicit to multi-material manufacturing schemes. The layer-by-layer nature of AM techniques can also facilitate the investigation of heterogeneous or *structured* electrodes with enhanced performance [42,43].

Acknowledgements

The authors would like to thank the UK Engineering and Physical Sciences Research Council (EPSRC) for financial support (grants EP/N509711/1, EP/P005411/1, EP/006566/1, EP/S001239/1 and EP/M009521/1), Robin Vincent and Gideon Ring for support in constructing the bespoke hybrid-AM machine, Andrew Lui for conducting the XRT scans.

Appendix

Supplementary data associated with this article can be found, in the online version, at https://doi.org/10.1016/j.addma.2019.05.001.

References

[1] X. Tian, J. Jin, S. Yuan, C.K. Chua, S.B. Tor, K. Zhou, Emerging 3D-printed electrochemical energy storage devices: a critical review, Adv. Energy Mater. 7 (17) (2017) 1700127, https://doi.org/10.1002/aenm.201700127.
[2] K.-H. Choi, D.B. Ahn, S.-Y. Lee, Current status and challenges in printed batteries: toward form factor-free, monolithic integrated power sources, ACS Energy Lett. 3 (1) (2018) 220–236, https://doi.org/10.1021/acsenergylett.7b01086.
[3] H. Hesse, M. Schimpe, D. Kucevic, A. Jossen, Lithium-ion battery storage for the grid-A review of stationary battery storage system design tailored for applications in modern power grids, Energies 10 (12) (2017) 2107, https://doi.org/10.3390/en10122107.
[4] B. Jacob, S.W. Ng, D.T. Wang, In Praise of Memory Systems: Cache, DRAM, Disk, Elsevier, 2008, https://doi.org/10.1016/B978-0-12-379751-3.50036-9.
[5] P. Simon, Y. Gogotsi, Materials for electrochemical capacitors, Nat. Mater. 7 (11) (2008) 845–854, https://doi.org/10.1038/nmat2297.
[6] B.E. Conway, Electrochemical Supercapacitors, Scientific Fundamentals and Technological Applications, Kluwer Academic, Plenum Publishers, New York, 1999.
[7] Y. Wang, Y. Song, Y. Xia, Electrochemical capacitors: mechanism, materials, systems, characterization and applications, Chem. Soc. Rev. 45 (21) (2016) 5925–5950, https://doi.org/10.1039/C5CS00580A.
[8 E. Frackowiak, Carbon materials for supercapacitor application, Phys. Chem. Chem. Phys. 9 (15) (2007) 1774, https://doi.org/10.1039/b618139m.
[9] G. Wang, L. Zhang, J. Zhang, A review of electrode materials for electrochemical supercapacitors, Chem. Soc. Rev. 41 (41) (2012) 797–828, https://doi.org/10.1039/c1cs15060j arXiv:1005.0853.
[10] M. Zhang, G. Wang, L. Lu, T. Wang, H. Xu, C. Yu, H. Li, W. Tian, Improving the electrochemical performances of active carbon-based supercapacitors through the combination of introducing functional groups and using redox additive electrolyte, J. Saudi Chem. Soc. 22 (8) (2018) 908–918, https://doi.org/10.1016/j.jscs.2018.02.001.
[11] C. Zhong, Y. Deng, W. Hu, J. Qiao, L. Zhang, J. Zhang, A review of electrolyte materials and compositions for electrochemical supercapacitors, Chem. Soc. Rev. 44 (21) (2015) 7484–7539, https://doi.org/10.1039/C5CS00303B.
[12] X. Peng, H. Liu, Q. Yin, J. Wu, P. Chen, G. Zhang, G. Liu, C. Wu, Y. Xie, A zwitterionic gel electrolyte for efficient solid-state supercapacitors, Nat. Commun. 7 (1) (2016) 11782, https://doi.org/10.1038/ncomms11782.
[13] F. Zhang, M. Wei, V.V. Viswanathan, B. Swart, Y. Shao, G. Wu, C. Zhou, 3D printing technologies for electrochemical energy storage, Nano Energy 40 (May) (2017) 418–431, https://doi.org/10.1016/j.nanoen.2017.08.037.
[14] I. Erlichman, Method for manufacturing flat batteries, (1976).
[15] H. Chadalavada, D.S. Raj, R.A. Kumar, K. Sankar, Production Lead Time Reduction in a Battery Manufacturing Unit using Lean Manufacturing, Int. J. Eng. Res. Technol. 4 (04) (2015) 842–847.
[16] Y. Shi, X. Zhou, G. Yu, Material and Structural Design of Novel Binder Systems for High-Energy, High-Power Lithium-Ion Batteries, Acc. Chem. Res. 50 (11) (2017) 2642–2652, https://doi.org/10.1021/acs.accounts.7b00402.
[17] W. Gao, N. Singh, L. Song, Z. Liu, A.L.M. Reddy, L. Ci, R. Vajtai, Q. Zhang, B. Wei, P.M. Ajayan, Direct laser writing of micro-supercapacitors on hydrated graphite oxide films, Nat. Nanotechnol. 6 (8) (2011) 496–500, https://doi.org/10.1038/nnano.2011.110.
[18] ASTM International, F2792-12a - Standard Terminology for Additive Manufacturing Technologies, Rapid Manufacturing Association (2013) 10-12arXiv:arXiv:1011.1669v3, doi:10.1520/F2792-12A.
[19] M. Hannibal, G. Knight, Additive manufacturing and the global factory: Disruptive technologies and the location of international business, Int. Bus. Rev. 27 (6) (2018) 1116–1127, https://doi.org/10.1016/j.ibusrev.2018.04.003.
[20] O.A. Mohamed, S.H. Masood, J.L. Bhowmik, Optimization of fused deposition modeling process parameters: a review of current research and future prospects, Adv. Manuf. 3 (1) (2015) 42–53, https://doi.org/10.1007/s40436-014-0097-7.
[21] T.D. Ngo, A. Kashani, G. Imbalzano, K.T. Nguyen, D. Hui, Additive manufacturing (3D printing): A review of materials, methods, applications and challenges, Compos. Part B: Eng. 143 (December 2017) (2018) 172–196, https://doi.org/10.1016/j.compositesb.2018.02.012.
[22] S. Singh, S. Ramakrishna, R. Singh, Material issues in additive manufacturing: A review, J. Manuf. Process. 25 (2017) 185–200, https://doi.org/10.1016/j.jmapro.2016.11.006.
[23] A. Saidi, L. Desfontaines, A. Champeval, J.-D. Lebreux, C. Lecomte, M. Pruneau, A. Grondein, R. Izquierdo, D. Bélanger, The effect of ink formulation and electrode geometry design on the electrochemical performance of a printed alkaline battery, Flexible and Printed Electronics 2 (1) (2017) 015002, https://doi.org/10.1088/2058-8585/aa56e8.
[24] K. Sun, T.-S. Wei, B.Y. Ahn, J.Y. Seo, S.J. Dillon, J.A. Lewis, 3D printing of interdigitated Li-ion microbattery architectures, Adv. Mater. 25 (33) (2013) 4539–4543, https://doi.org/10.1002/adma.201301036.
[25] M. Attaran, Additive manufacturing: the most promising technology to alter the supply chain and logistics, J. Service Sci. Manag. 10 (03) (2017) 189–206, https://doi.org/10.4236/jssm.2017.103017.
[26] A. Ambrosi, M. Pumera, 3D-printing technologies for electrochemical applications, Chem. Soc. Rev. 45 (10) (2016) 2740–2755, https://doi.org/10.1039/C5CS00714C.
[27] D. Zhang, B. Chi, B. Li, Z. Gao, Y. Du, J. Guo, J. Wei, Fabrication of highly conductive graphene flexible circuits by 3D printing, Synth. Met. 217 (2016) 79–86, https://doi.org/10.1016/j.synthmet.2016.03.014.
[28] W. Yu, H. Zhou, B.Q. Li, S. Ding, 3D Printing of Carbon Nanotubes-Based Microsupercapacitors, ACS Appl. Mater. Interf. 9 (5) (2017) 4597–4604, https://doi.org/10.1021/acsami.6b13904.
[29] M. Wei, F. Zhang, W. Wang, P. Alexandridis, C. Zhou, G. Wu, 3D direct writing fabrication of electrodes for electrochemical storage devices, J. Power Sources 354 (2017) 134–147, https://doi.org/10.1016/j.jpowsour.2017.04.042.
[30] B.N. Turner, R. Strong, S.A. Gold, A review of melt extrusion additive manufacturing processes: I. Process design and modeling, Rapid Prototyping J. 20 (3) (2014) 192–204, https://doi.org/10.1108/RPJ-01-2013-0012.
[31] K.V. Wong, A. Hernandez, A Review of Additive Manufacturing, ISRN Mechanical Engineering 2012 (2012) 1-10. arXiv:208760, doi:10.5402/2012/208760.
[32] K. Hon, L. Li, I. Hutchings, Direct writing technology-Advances and developments, CIRP Ann. 57 (2) (2008) 601–620, https://doi.org/10.1016/j.cirp.2008.09.006.
[33] J. Cesarano, A Review of Robocasting Technology, MRS Proceedings 542 (1998) 133, https://doi.org/10.1557/PROC-542-133.
[34] Y. Lin, F. Liu, G. Casano, R. Bhavsar, I.A. Kinloch, B. Derby, Pristine graphene aerogels by room-temperature freeze gelation, Adv. Mater. 28 (36) (2016) 7993–8000, https://doi.org/10.1002/adma.201602393.

[35] J. G. Ziegler, N. B. Nichols, Optimum Settings for Automatic Controllers, Transactions of the A.S.M.E.doi:10.1115/1.2899060. URL http://dynamicsystems.asmedigitalcollection.asme.org/article.aspx?articleid=1406231.
[36] A. Kraytsberg, Y. Ein-Eli, Conveying advanced li-ion battery materials into practice the impact of electrode slurry preparation skills, Adv. Energy Mater. 6 (21) (2016) 1600655, https://doi.org/10.1002/aenm.201600655.
[37] Z. Zhu, Effects of Various Binders on Supercapacitor Performances, Int. J. Electrochem. Sci. 11 (10) (2016) 8270–8279, https://doi.org/10.20964/2016.10.04.
[38] S. Zhang, N. Pan, Supercapacitors Performance Evaluation, Advanced Energy Materials 5 (6). doi:10.1002/aenm.201401401. URL http://doi.wiley.com/10.1002/aenm.201401401.
[39] B.-A. Mei, O. Munteshari, J. Lau, B. Dunn, L. Pilon, Physical Interpretations of Nyquist Plots for EDLC Electrodes and Devices, J. Phys. Chem. C 122 (1) (2018) 194–206., https://doi.org/10.1021/acs.jpcc.7b10582.
[40] R.P. Chhabra, Non-Newtonian Fluids: An Introduction, in: Rheology of Complex Fluids, Springer New York, New York, NY, 2010, pp. 3–34, https://doi.org/10.1007/978-1-4419-6494-6_1.
[41] F. Beguin, Supercapacitors - Materials, Systems, and Applications, Wiley-VCH Verlag GmbH & Co, KGaA, 2013, https://doi.org/10.1002/9783527646661.
[42] C. Huang, J. Zhang, N.P. Young, H.J. Snaith, P.S. Grant, Solid-state supercapacitors with rationally designed heterogeneous electrodes fabricated by large area spray processing for wearable energy storage applications, Sci. Reports 6 (1) (2016) 25684, https://doi.org/10.1038/srep25684.
[43] R. Drummond, C. Huang, P. S. Grant, Overcoming diffusion limitations in supercapacitors using layered electrodes, Journal of Power Sources, https://doi.org/10.1016/j.jpowsour.2019.04.107.